Design of highly-sinterable LATP-CNT composite powder by sequential particle assembly for fabrication of highly electrical-conductive composite electrodes

Kento Ishii [a*], Atsushi Yokoi [c], Yusaku Sato [b], Kazuhiro Hikima [b], Go Kawamura [b], Wai Kian Tan [b], Hiroyuki Muto [b*], Atsunori Matsuda [b], Tetsuo Uchikoshi [d*], Masayoshi Fuji [a]

[a] *Nagoya Institute of Technology, Advanced Ceramics Research Center, 3-101-1 Honmachi, Tajimi, Gifu, 507-0033, Japan*

[b] *Toyohashi University of Technology, 1-1 Hibarigaoka, Tempaku-cho, Toyohashi, Aichi, 441-8580, Japan*

[c] *National Institute of Technology (KOSEN), Numazu College, 3600 Ooka, Numazu, Shizuoka, 410-8501, Japan*

[d] *National Institute for Material Science, 1-2-1 Sengen, Tsukuba, Ibaraki 305-0047, Japan*

*Corresponding author.

Email address: ishii.kento@nitech.ac.jp (K. Ishii)

Email address: muto@ee.tut.ac.jp (H. Muto)

Email address: UCHIKOSHI.Tetsuo@nims.go.jp (T. Uchikoshi)

Abstract

A sequential particle assembling process was developed to fabricate composite particles with multiple components. Cobalt sintering aids and carbon nanotube (CNT) conductive additives were sequentially and electrostatically absorbed on $Li_{1.3}Al_{0.3}Ti_{1.7}(PO_4)_3$ (LATP) electrolyte particles under various dispersion conditions. The effect of the particle assembling conditions on the composite body's sintering ability and conductive properties was investigated. By optimizing the microstructure of the composite particle and its particle charging conditions, it became possible to obtain a sintered composite electrode with a finely connected path of each LATP and CNT phase.

Keywords: Sequential particle assembly, Composite, LATP, CNT, LCP

1. Introduction

The properties of composite materials are not solely determined by the mixing ratio, but are also significantly affected by their microstructure, such as the dispersion state of each phase and the morphology of the added particles. Some research has reported more advanced organizational structures, such as multiscale periodic regular self-organization, fractals, and hierarchical structures [1,2]. Particle assembly technology is an approach that can realize these structures from the bottom up from nano to micro to macro scale [3,4]. Among the particle assembly techniques, electrostatic assembly (EA), which utilizes the charging of particles in a colloidal solution, is a promising method [5–9]. This method can electrostatically integrate positively and negatively charged particles into a composite particle. Composite particles can be made into large monodisperse spherical particles that are easy to handle and can be used as a basic unit to create a periodic three-dimensional structure. Composites produced using this method have further improved mechanical, electrical, and thermal properties [7–14].

In all-solid-state batteries, the electrode is composed of multiple phases; i.e., an ion-conducting phase, an electron-conducting phase, and an electrode-active material. A composite electrode consisting of an active material, a conductive agent (electronic conductor), and an electrolyte material (ionic conductor) is used to ensure the conductivity of both the Li-ions and electrons in the electrode [15–19]. The preferred composite electrode microstructure for improving the transport rate of each carrier and reducing the effective thickness is the percolated structure (co-continuous structure) of each phase. However the microstructural control of the composites consisting of various components is very difficult and advanced structure control technology is required. The EA method is suitable as a method for manufacturing composite electrodes that allow each phase in the structure to be appropriately arranged, and is expected to improve the battery characteristics. The NASICON-type $Li_{1.3}Al_{0.3}Ti_{1.7}(PO_4)_3$ (LATP) is a promising oxide-based electrolyte material with an excellent lithium ion conductivity, low cost, low toxicity, good electrochemical stability and easy synthesis [20–23]. Many oxide-based electrolytes have a low chemical stability against air and water, but LATP has a high stability against these, thus the colloid process can be applied. Aqueous solvents have many advantages over nonaqueous solvents, including a greater polarity, the ability to use a variety of surfactants, and easier dispersion control. Therefore, surface modification by the colloidal process can be effectively applied.

In a previous study, composite particles consisting of the LATP electrolyte material, Carbon nanotube (CNT) conductive additive, and Ni-Mn-Co-based cathode active material were prepared using the EA method, and their electrical properties were evaluated [24]. However, detailed experimental conditions have not been investigated regarding the influence of the process factors for particle compositing, such as particle charging and the amount of dispersant, on the properties. Furthermore, co-modification of a sintering aid and an electron conductive aid has not been studied. It is expected that by examining the process conditions in more detail, it will be possible to design solid electrolyte particles that have both a good sintering ability and electronic conductivity. We have reported that low-

temperature sintering of LATP electrolytes are enabled by cobalt surface modification [25–27]. In this study, the electrostatic dispersion of the Co-modified LATP and CNTs was controlled, and composite particles were prepared by combining them under various dispersion conditions, which were not considered in the previous report. Finally, the influence of the particle composite conditions on the sintering ability and conductive properties of the LATP is discussed.

2. Experimental methods

Surface modification of LATP with Co was performed according to the procedure from previous research [25,26]. Commercially-available LATP powder (Particle size of 1μm>, Toshima Manufacturing Co., Ltd.) and cobalt nitrate hexahydrate ($Co(NO_3)_2 \cdot 6H_2O$, Kanto Chemical Co., Inc.) were used for the experiments. The morphology of the as-received LATP particles is shown in Fig. S1(a). The weighed cobalt nitrate hexahydrate was first dissolved in water. While the solution was being ultrasonicated, 15 vol% LATP powder was added to this solution. The LATP with *x* wt% Co of cobalt nitrate was denoted as "Co*x*-LATP".

Figure 1 shows a schematic diagram of the Co-LATP and CNT compositing process by the electrostatic adsorption method. PDDA [Poly(diallyldimethylammonium chloride), average molecular weight of ~100,000-200,000, Sigma-Aldrich Co. LLC], a polycationic dispersant, was diluted 100 times with water and used as a dispersant for the LATP. After adding a predetermined amount of PDDA to the LATP weight under ultrasonication, the slurry was diluted with distilled water so that the total amount of the slurry was 50 ml. CNT (Single-wall carbon nanotube, average diameter of 2 nm and average length of 1μm, TUBALL™, OCSiAl Co., Ltd.) of a given weight ratio to LATP was weighed and added to 50 ml of distilled water. SDC (Sodium deoxycholate, average molecular weight of 415, FUJIFILM Wako Pure Chemical Co., Ltd.), an anionic dispersant, was diluted 100 times with water and used as a

dispersant for the CNT. The morphology of the as-received CNT is shown in Fig. S1(b). A predetermined amount of the SDC dispersant, relative to the weight of the CNTs, was added to the CNT slurry. The CNT slurry was sonicated for 1 h for defibration and dispersion using an ultrasonication generator (model us-1200, Sonic Technology Co., Ltd.). At this time, to prevent the CNT slurry from heating, the slurry beaker was placed in a stainless-steel vat filled with ice water, and the treatment was performed while cooling as shown in Fig.S2. The dispersed CNT slurry and the Co-LATP slurry were mixed, and the composite particles were formed. Co*x*-LATP with *y*wt% CNT was labeled "(Co*x*-LATP)-CNT*y*". The mixed slurry was dried in an oven at 50 °C, and the powder mass of the composite particles was collected. The collected coarse powder was crushed using an agate mortar. The powder was then mixed with LCP powder (Particle size of 5-10μm, Toshima Manufacturing Co., Ltd.). The morphology of the as-received LCP powder is shown in Fig. S1(c). The powder was uniaxially pressed at 100 MPa into a disc shape with a 10-mm diameter and 2-mm thickness. The obtained compact was sintered in an Ar atmosphere at 400 °C as the 1st step and at 800 °C as the 2nd step by a two-step sintering method, according to a previous study [27]. The zeta potentials of the slurries were measured by laser doppler velocimetry (Zetasizer Nano-ZS, Malvern Instruments, UK). The zeta potential of the aqueous slurries was calculated by applying Smoluchowski's equation. The relative densities (RD) of the samples were calculated based on the bulk density and theoretical density. The theoretical density of the composite was determined by considering the theoretical densities of the Co-LATP and CNTs and their mixing ratio.

The microstructures of the samples were observed by a scanning electron microscope (SEM) (JSM-6500F and JSM-7600F, JEOL Ltd., Japan). The fired composite pellets were polished using sandpaper and coated with Au electrodes on both sides using a sputtering apparatus (SC-701, Sanyu Electronics Co., Ltd., Japan). The DC electrical conductivities of the Au-coated samples were measured at room temperature using a source meter (Model 2410, Keithley Instruments, Inc., US).

3. Results & Discussion

Figure 2 shows the effect of the addition of cobalt nitrate hexahydrate on the zeta potential of the LATP suspension. The zeta potential of LATP increased with the increasing Co addition at $x = 0.0$ to 2.0 It has been reported that $x = 0.3$~0.5 is the optimum value for the cobalt addition to achieve both a high density and high conductivity of LATP [25,27]. In this study, the Co addition of $x = 0.3$ was selected, which minimizes the effect of the zeta potential in different solvents. The sintering density of Co-LATP was more than 80% for $x = 0.3$ in an aqueous solvent, which is similar to that in the ethanol solvent. A change in the LATP color from white to pink was observed in water as well as in the ethanol solvent indicating adsorption of the cobalt nitrate ions on the LATP. Figure 3 shows the effect of the addition of nitric acid and cobalt nitrate hexahydrate on the pH and zeta potential of the LATP slurry. The pH and zeta potential decreased by the addition of nitric acid. On the other hand, when cobalt nitrate hexahydrate was added, the pH changed to about 6 and remained constant. For the cobalt nitrate additions of $x = 0$ to 0.3, the pH change (from 7 to 6) and the zeta potential decrease (from -50 mV to -43 mV) are not severe, so the presence or absence of the cobalt nitrate addition to LATP is not expected to have a significant effect on the subsequent particle compositing process. It is understood that the zeta potential enhancement due to the addition of cobalt nitrate is not an effect of the pH change. The following experimental results discuss the results obtained with the cobalt-modified LATP at $x = 0.3$ (Co0.3-LATP).

Figure 4 shows the effect of the PDDA addition to the LATP/water slurry on the zeta potential. LATP is initially negatively charged with a zeta potential of about -50 mV. The zeta potential is significantly changed, and the charge is reversed from negative to positive by adding 1 wt% PDDA. The zeta potential significantly increases in a more positive direction up to 3 wt% addition, but above 3 wt%, the zeta potential does not significantly increase. The significant change in the zeta potential up to 3 wt%

indicates that PDDA is in the process of adsorbing on the LATP particle surface. The slight change in the zeta potential above 3 wt% suggests saturation of the PDDA adsorption on the LATP surface and the presence of excess PDDA. The intersection of the onset and offset lines of the zeta potential curve was considered to be the adsorption saturation point at which PDDA adsorbs on LATP without any excess or deficiency, and the value was 2 wt%.

Figure 5 shows the relationship between the amount of added SDC and the zeta potential in the CNT aqueous suspensions. After preparing the CNT slurry, the CNTs formed clusters of entangled bundles, and as reported in previous studies, the slurry was clearly separated into a liquid phase and a CNT phase, each of which could be visually identified [9]. With the addition of 10 wt% to 100 wt% SDC, the zeta potential significantly improved, and no CNT clusters were observed in the slurry. The zeta potential did not change from 100 wt% to 1000 wt% SDC addition. The intersection of the onset and offset lines of this curve at 10 wt% to 1000 wt% was approximately 100 wt%. 100 wt% was regarded as the adsorption saturation point where SDC is adsorbed on the CNTs without any excess or deficiency. Based on these results, the optimal addition amounts of PDDA and SDC were determined to be 2 wt% and 100 wt%, respectively. The zeta potential neutralization behavior of PDDA with SDC was evaluated by the addition of SDC to 2 wt% PDDA-modified LATP, as shown in Fig. S3. The zeta potential did not change up to 3wt% SDC addition, but the zeta potential significantly changed above 3wt%. The zeta potential turned from positive to negative at 40 wt% SDC addition, then the zeta potential negatively increased. The positive charge of PDDA was counteracted by the negative charge of SDC up to 3 wt% addition, but the PDDA was still dominant due to the small amount of added SDC. From the addition of 3 wt% or more, the neutralization of the PDDA charge becomes more pronounced, and finally the modification of SDC on PDDA is completed at 40 wt% and its charge turned negative. The monomer molecular weight of PDDA is 161 and the SDC molecular weight is 415, and since they are monovalent ions, if they were to completely neutralize each other by equal weight, two to three times as much SDC would

be needed relative to PDDA. This is postulated to be due to the adsorption of PDDA on the surface of the LATP particles, differences in the degree of ionization and other factors. An excess SDC-modified CNT would not uniformly form complexes with the PDDA-modified LATP, resulting in a nonhomogeneous microstructure.

Figure 6 shows the particle morphology of the (Co0.3-LATP)-CNT1.0 composite powder without a dispersant and the (Co0.3-LATP)-CNT1.0 composite powder with the determined dispersant addition. In the composite powder with no added dispersant, the CNT bundles were not disentangled, and the bundles were relatively thick. Also, the LATP particles and CNT bundles do not appear to be intentionally attached. On the other hand, in the composite powder with the added dispersant, the CNTs were much finer than those without the dispersant, and the bundles were well disentangled. Furthermore, many LATP particles appeared to be attached to the CNT bundles by electrostatic interactions.

The length of CNT is much longer than the particle size of LATP. Depending on the compositing conditions, it is assumed that composite particles are formed in which multiple Co-LATP particles are adsorbed like grapes on the CNT bundles. The magnitude of the electrostatic interaction varies depending on the strength of the zeta potential between Co-LATP and CNT, which would affect the structure of the composite particles, the size and packing density as shown in Fig. S4.

As the amount of the added SDC dispersant increases, the CNTs become more negatively charged while becoming disentangled. As the amount of the added PDDA dispersant increases, Co-LATP reverses from a negative charge to positive charge and becomes more positively charged. CNT and Co-LATP repeatedly adsorb each other, and the composite particles grow larger until either the positive or negative charge is neutralized. The balance of surface charges between the Co-LATP and CNT significantly impacts the particle compositing. The number of particles required to neutralize each charge and the size of the particles formed vary depending on the strength of the surface charge. Figure 6(b) shows an example of the composite particles that grew particularly large, but such coarse particles

were not in high enough numbers to affect the overall sinterability.

The greater the electrostatic interaction force, the denser and smaller the composite particles formed. The weaker the force, the coarser and larger the composite particles formed. When bulk bodies are observed on a macroscopic scale, small, dense composite particles are localized as clusters throughout the sample. When the amount of added CNT is extremely small, it is advantageous for forming a percolation structure over a short distance, but is not suitable for forming a percolation structure over a long distance. The conditions for forming composite particles, such as the amount of added CNT and the combination of the zeta potential, must be optimized according to the desired bulk size.

Figure ~~8~~ 7 shows the fracture surfaces of the Co-LATP and CNT composite after firing (a) without adding PDDA and SDC (The CNT parts are indicated by the red arrows.), and (b) with 2wt%-PDDA and 100wt%-SDC. In all the samples, the CNTs were maintained without burning after firing, and necks were formed between the LATP particles. The amount of the added CNT in this study was very small, and the amount of added Co-LATP was quite large. Since the gaps between the composite particles are filled with Co-LATP, it is postulated that the structure changes due to the composite particles' collapse before and after uniaxial pressing are not very significant. In the sample with no added dispersant, clumps of the CNTs were observed in the microstructure. In addition, thick CNT bundles in the structure were observed in the higher magnification images. In the microstructures of the dispersant-added samples shown in Fig. ~~8~~ 7 (b), no CNT clumps or thick bundles were observed at low and medium magnifications. In the high-magnification tissue, the fine CNT fibers were uniformly dispersed.

Figure ~~9~~ 8 shows the relative density of Co0.3-LATP with various CNT amounts before and after firing. The sintered density without CNT addition was over 80%, and the sintered density of any CNT-added Co-LATP was less than 70% over the CNT amount of 1.0 wt%, similar to the green density. Carbon materials are generally difficult to sinter, so the carbon phase inhibits the sintering of the LATP phase. In other words, a high CNT dispersion in the composite structure reduces the contact points

between the LATP particles and inhibits the sintering of the LATP phase, resulting in the decreased sintered density. This is a good result, suggesting that each LATP particle is modified with CNT which serves as an electron conduction path. Although the apparent sintered density was not high, necks were formed between the LATP particles, and the hardness of the sample when broken for SEM observation was closer to that of a sintered unmodified LATP rather than a compact. This is another important result, suggesting that a sufficient conduction path for Li ions is developed in the region not covered by the CNTs. The samples refer to the specimen whose fracture surface was observed by SEM in Figure ~~8~~ 7. When changing not only the zeta potential but also the amount of added CNT, there are many more factors to consider regarding the composite hardness, such as the size of the composite particles, the filling rate and the reinforcement effect. In this study, the amount of added CNT was small, so there was no significant difference in the strength due to the difference in the CNT amount.

Figure ~~10~~ 9 shows the electrical conductivity of the (Co0.3-LATP)-CNT fired bodies with various CNT additions under the addition conditions of 2 wt%-PDDA and 100 wt%-SDC. The conductivity of Co-LATP without the CNTs is 6.50×10^{-6} S/cm, and that of Co-LATP with 1.0 wt% CNTs is 3.77×10^{-2} S/cm, an approximate three orders of magnitude higher value. This increase in conductivity can be attributed to the electronic conductivity of the CNT phase. The sharp increase in the electrical conductivity between 0.0 wt% and 1.0 wt% CNT addition suggests that the CNT percolation threshold is at or below 0.5 wt%. The electrical conductivity also linearly increased with the increasing CNT content from 0.5 wt% or more. The electrical conductivity of the (Co0.3-LATP)-CNT1.0 sintered bodies prepared with different dispersant additions is shown in Fig. ~~S4~~ S5. The highest conductivity was obtained at the optimized dispersant additions of 2 wt% PDDA and 100 wt% SDC. The second highest conductivity was observed when no dispersant was added, possibly because the aggregated thick CNT bundles are inherently less electrically resistant than the fine CNT fibers and have a longer fiber length. These results suggest a complex correlation between the CNT morphology and dispersion and electrical

conductivity. Finally, this correlation is expected to affect the battery characteristics.

The $LiCoPO_4$ (LCP) electrode active material, reported to be chemically compatible with LATP, was composited into an optimized (Co-LATP)-CNT composition [26]. Fig. ~~11~~ 10 shows the fracture surfaces of various composites after firing; (a) 70vol%-LATP with 30vol%-LCP, (b) Co0.3-LATP with 0.5wt%-CNT, and (c) 70vol%-(Co0.3LATP with 0.5wt%-CNT) with 30vol%-LCP. In addition, the relative densities and electrical conductivities are shown in Table 1. The composite with LCP improved the sinterability of the LATP phase and succeeded in achieving both a high dispersion of the CNT phase and high densification of the oxide phases. Finally, this process is beneficial for the microstructure control of the multi-component material, and the composite material fabricated by this method is also expected to show an excellent performance for composite electrodes.

Conclusions

The Co-LATP electrolyte and CNT conductive aid were positively and negatively charged using a dispersant, respectively, and electrostatically composited. The CNTs in the composite powder prepared using the optimal amount of dispersant are well disentangled and dispersed in the matrix, and the conductivity of the composite after firing is improved compared to the composite without a using dispersant. Uniformly modified CNTs sterically prevented contact between the Co-LATP particles resulting in the inhibition of densification. Nevertheless, it was confirmed that the addition of Co reliably formed bonds between the LATPs in areas where the CNTs were not present. In this way, when using CNTs as an electron conduction aid, it is effective to design the surface so that all the LATP electrolyte particles are in partial contact with the CNTs, while sintering is promoted elsewhere. The assembled (Co-LATP)-CNT-LCP powder showed an excellent compatibility of sintering and electrical properties. The sequential particle assembling process for the electrolyte, sintering aid, and conductive additive and

active material, is very promising as a manufacturing technology for composite electrodes used in all-solid-state batteries.

Acknowledgments

We would like to thank Dr. Shoji Yamaguchi at NIMS for his valuable comments in carrying out the research. This study was supported in part by the Materials Processing Science Project ("Materealize"), grant number JPMXP0219207397 from MEXT.

References

[1] P. Fratzl, R. Weinkamer, Nature's hierarchical materials, Prog. Mater. Sci. 52 (2007) 1263–1334. https://doi.org/10.1016/j.pmatsci.2007.06.001.

[2] F. Munakata, M. Takeda, K. Nemoto, K. Ookubo, Y. Sato, Y. Mizukami, M. Koga, S. Abe, Y. Bao, R. Kobayashi, Multifractal characteristics of the self-assembly material texture of β-Si3N4/SUS316L austenitic stainless steel composites, J. Alloys Compd. 853 (2021) 156570. https://doi.org/10.1016/j.jallcom.2020.156570.

[3] K. Ariga, T. Nakanishi, J.P. Hill, Self-assembled microstructures of functional molecules, Curr. Opin. Colloid Interface Sci. 12 (2007) 106–120. https://doi.org/10.1016/j.cocis.2007.05.008.

[4] K. Zhang, M. Jiang, D. Chen, Self-assembly of particles - The regulatory role of particle flexibility, Prog. Polym. Sci. 37 (2012) 445–486. https://doi.org/10.1016/j.progpolymsci.2011.09.003.

[5] E. Guzmán, R.G. Rubio, F. Ortega, A closer physico-chemical look to the Layer-by-Layer electrostatic self-assembly of polyelectrolyte multilayers, Adv. Colloid Interface Sci. 282 (2020) 102197. https://doi.org/10.1016/j.cis.2020.102197.

[6] F. Caruso, H. Lichtenfeld, M. Giersig, R. Chaussee, D.- Berlin, G. Strasse, R. V May,

Electrostatic Self-Assembly of Silica Nanoparticle - Polyelectrolyte Multilayers on Polystyrene Latex Particles Max-Planck-Institute of Colloids and Interfaces The area of thin film fabrication , in which ordered , functional supramolecular structures are, J. Am. Chem. Soc. 120 (1998) 8523–8524.

[7] A. Yokoi, W.K. Tan, T. Kuroda, G. Kawamura, A. Matsuda, H. Muto, Design of heat-conductive hBN–PMMA composites by electrostatic nano-assembly, Nanomaterials. 10 (2020). https://doi.org/10.3390/nano10010134.

[8] H. Muto, A. Yokoi, W.K. Tan, Electrostatic assembly technique for novel composites fabrication, J. Compos. Sci. 4 (2020). https://doi.org/10.3390/jcs4040155.

[9] H. Muto, Y. Sato, W.K. Tan, A. Yokoi, G. Kawamura, A. Matsuda, Controlled formation of carbon nanotubes incorporated ceramic composite granules by electrostatic integrated nano-assembly, Nanoscale. 14 (2022) 9669–9674. https://doi.org/10.1039/d2nr01713j.

[10] W.K. Tan, K. Tsuzuki, A. Yokoi, G. Kawamura, A. Matsuda, H. Muto, Formation of porous Al2O3–SiO2 composite ceramics by electrostatic assembly, J. Ceram. Soc. Japan. 128 (2020) 605–610. https://doi.org/https://doi.org/10.2109/jcersj2.20064.

[11] N.H.H. Phuc, M. Takaki, H. Muto, M. Reiko, H. Kazuhiro, A. Matsuda, Sulfur-Carbon Nano Fiber Composite Solid Electrolyte for All-Solid-State Li-S Batteries, ACS Appl. Energy Mater. 3 (2020) 1569–1573. https://doi.org/10.1021/acsaem.9b02062.

[12] W.K. Tan, T. Kuwana, A. Yokoi, G. Kawamura, A. Matsuda, H. Muto, Electrostatically assembled SiC–Al_2O_3 composite particles for direct selective laser sintering, Adv. Powder Technol. 32 (2021) 2074–2084. https://doi.org/https://doi.org/10.1016/j.apt.2021.04.018.

[13] W.K. Tan, Y. Araki, A. Yokoi, G. Kawamura, A. Matsuda, H. Muto, Micro- and Nano-assembly of Composite Particles by Electrostatic Adsorption, Nanoscale Res. Lett. 14 (2019) 1–9. https://doi.org/10.1186/s11671-019-3129-1.

[14] W.K. Tan, Y. Matsubara, A. Yokoi, G. Kawamura, A. Matsuda, I. Sugiyama, N. Shibata, Y. Ikuhara, H. Muto, Transparent conductive polymer composites obtained via electrostatically assembled carbon nanotubes–poly (methyl methacrylate) composite particles, Adv. Powder Technol. 33 (2022) 103528. https://doi.org/10.1016/j.apt.2022.103528.

[15] N. Ogihara, Y. Itou, T. Sasaki, Y. Takeuchi, Impedance spectroscopy characterization of porous electrodes under different electrode thickness using a symmetric cell for high-performance lithium-ion batteries, J. Phys. Chem. C. 119 (2015) 4612–4619. https://doi.org/10.1021/jp512564f.

[16] C. Araki, S. Tsubouchi, A. Noie, E. Nishimura, J. Kawaji, S. Suzuki, Thickness Dependence of Resistance Components of a $LiNi_xCo_yMn_{1-x-y}O_2$-Based Positive Electrode for Lithium Ion Batteries , J. Electrochem. Soc. 168 (2021) 040503. https://doi.org/10.1149/1945-7111/abf0d9.

[17] P. Braun, C. Uhlmann, M. Weiss, A. Weber, E. Ivers-Tiffée, Assessment of all-solid-state lithium-ion batteries, J. Power Sources. 393 (2018) 119–127. https://doi.org/10.1016/j.jpowsour.2018.04.111.

[18] G.F. Dewald, S. Ohno, J.G.C. Hering, J. Janek, W.G. Zeier, Analysis of Charge Carrier Transport Toward Optimized Cathode Composites for All-Solid-State Li−S Batteries, Batter. Supercaps. 4 (2021) 183–194. https://doi.org/10.1002/batt.202000194.

[19] D. Cao, Y. Zhao, X. Sun, A. Natan, Y. Wang, P. Xiang, W. Wang, H. Zhu, Processing Strategies to Improve Cell-Level Energy Density of Metal Sulfide Electrolyte-Based All-Solid-State Li Metal Batteries and beyond, ACS Energy Lett. 5 (2020) 3468–3489. https://doi.org/10.1021/acsenergylett.0c01905.

[20] X. Lu, R. Wang, F. Zhang, J. Li, The influence of phosphorous source on the properties of NASICON lithium-ion conductor $Li_{1.3}Al_{0.3}Ti_{1.7}(PO_4)_3$, Solid State Ionics. 354 (2020) 115417. https://doi.org/10.1016/j.ssi.2020.115417.

[21] K. Yang, L. Chen, J. Ma, Y. He, F. Kang, Progress and perspective of $Li_{1+x}Al_xTi_{2-x}(PO_4)_3$ ceramic electrolyte in lithium batteries, InfoMat. 3 (2021) 1195–1217. https://doi.org/10.1002/inf2.12222.

[22] H. Aono, E. Sugimoto, N. Imanaka, G. Adachi, Ionic Conductivity of Solid Electrolytes Based on Lithium Titanium Phosphate, J. Electrochem. Soc. 137 (1990) 1023–1027.

[23] J.A. Dias, S.H. Santagneli, Y. Messaddeq, Methods for Lithium Ion NASICON Preparation: From Solid-State Synthesis to Highly Conductive Glass-Ceramics, J. Phys. Chem. C. 124 (2020) 26518–26539. https://doi.org/10.1021/acs.jpcc.0c07385.

[24] K. Hikima, Y. Sato, A. Yokoi, W.K. Tan, H. Muto, A. Matsuda, Fabrication and electrochemical properties of electrode composites for oxide-type all-solid-state batteries through electrostatic integrated assembly, Heliyon. 9 (2023) e17889. https://doi.org/10.1016/j.heliyon.2023.e17889.

[25] K. Ishii, M. Ode, K. Mitsuishi, S. Miyoshi, T. Ohno, K. Takada, T. Uchikoshi, Effect of cobalt addition to NASICON-type $Li_{1.3}Al_{0.3}Ti_{1.7}(PO_4)_3$ (LATP) on its sintering behavior and electrical properties, J. Power Sources. 546 (2022) 1–8. https://doi.org/10.1016/j.jpowsour.2022.231954.

[26] K. Ishii, T. Uchikoshi, S. Miyoshi, M. Ode, T. Ohno, K. Takada, Reactivity evaluation of NASICON-type solid electrolyte LATP , LAGP and Olivine-type cathode LCP, Mater. Lett. 324 (2022) 132736. https://doi.org/10.1016/j.matlet.2022.132736.

[27] K. Ishii, T. Uchikoshi, K. Takada, Low-temperature sintering of $Li_{1.3}Al_{0.3}Ti_{1.7}(PO_4)_3$ electrolytes enabled by cobalt surface modification followed by two-step sintering, J. Ceram. Soc. Japan. 131 (2023) 298–305. https://doi.org/10.2109/jcersj2.23059.

Figure Captions

Fig. 1 Schematic illustration of the electrostatic integration method for LATP and CNT.

Fig. 2 The zeta potential of cobalt-added LATP in water as the solvent.

Fig. 3 Effect of addition of HNO_3 and $Co(NO_3)_2 \cdot 6H_2O$ to the LATP/water on the pH and zeta potential

Fig. 4 The zeta potential of the LATP with varying PDDA addition amounts.

Fig. 5 The zeta potential of the CNT with varying SDC addition amounts.

Fig. 6 Morphologies of the Co0.3-LATP and CNT composite powder at different magnifications (a) without adding PDDA and SDC, (b) with 2wt%-PDDA and 100wt%-SDC (The CNT parts are indicated by the red arrows.).

Fig. 7 The fracture surfaces of the Co0.3-LATP and CNT composite after firing (a) without adding PDDA and SDC (The CNT parts are indicated by the red arrows.), (b) with 2wt%-PDDA and 100wt%-SDC.

Fig. 8 The relative densities of the Co0.3-LATP and CNT composite before and after firing.

Fig. 9 The electrical conductivity of the (Co0.3-LATP)-CNT fired bodies with various CNT additions under the addition conditions of 2 wt% PDDA and 100 wt% SDC.

Fig. 10 The fracture surfaces of various composites after firing (a) 70vol%-LATP with 30vol%-LCP, (b) Co0.3-LATP with 0.5wt%-CNT, (c) 70vol%-(Co0.3-LATP with 0.5wt%-CNT) and with 30vol%-LCP.

Table 1 The relative density and electrical conductivity of 70vol%-LATP with 30vol%-LCP, Co0.3LATP with 0.5wt%-CNT and 70vol%-(Co0.3LATP with 0.5wt%-CNT) and with 30vol%-LCP.

Fig.1

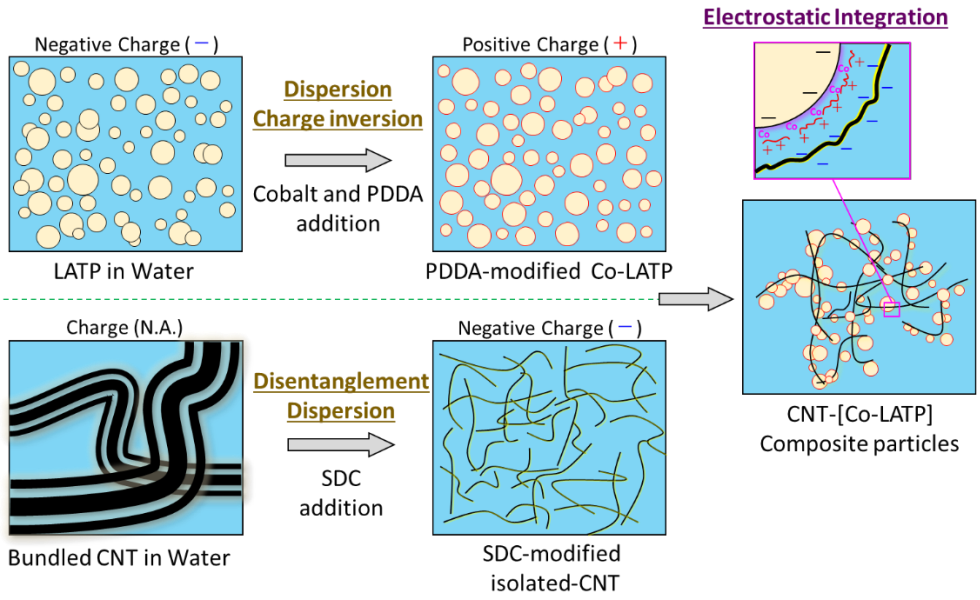

Fig. 1. Schematic illustration of the electrostatic integration method for LATP and CNT.

Fig.2

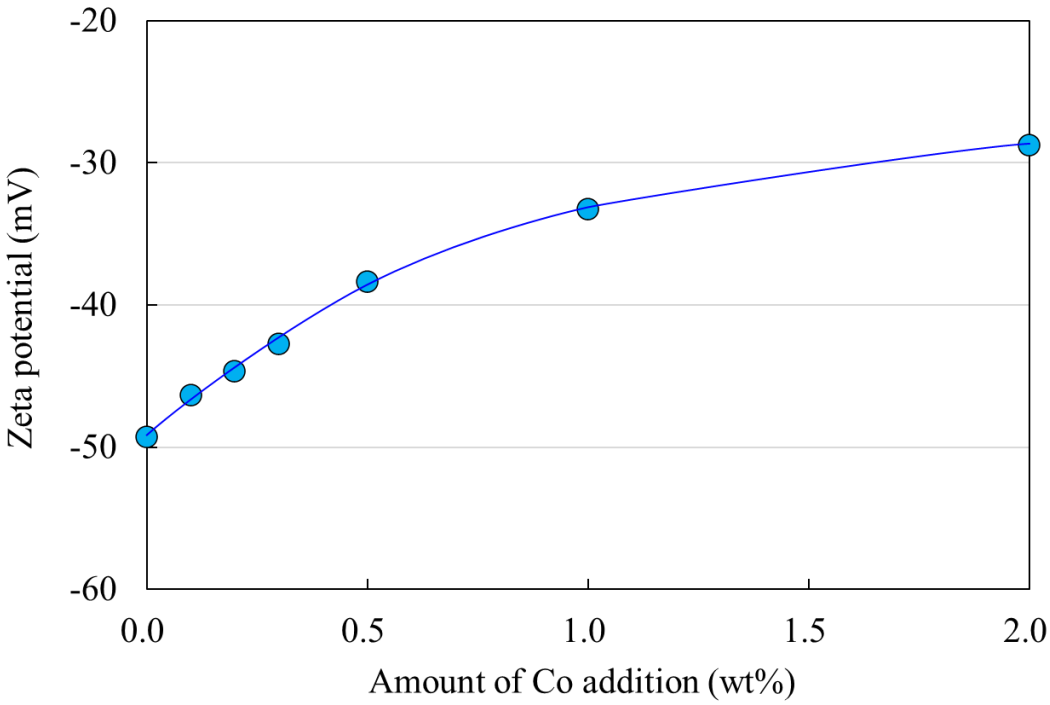

Fig. 2. The zeta potential of cobalt-added LATP in water as the solvent.

Fig.3

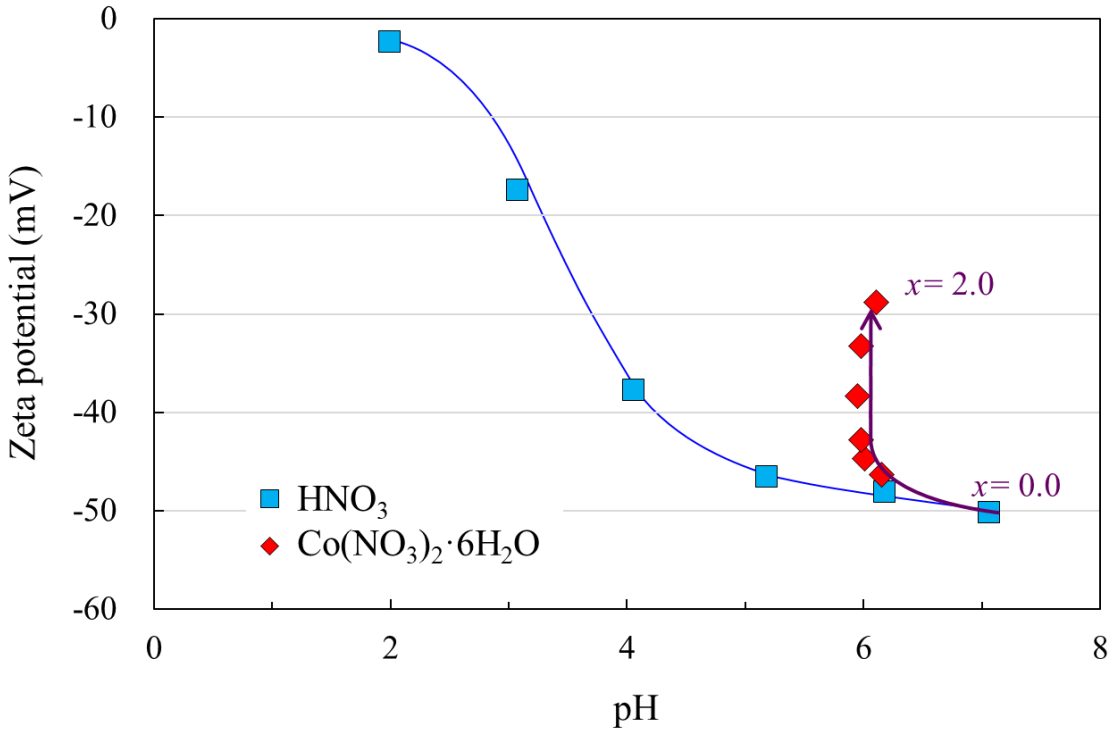

Fig. 3. Effect of addition of HNO_3 and $Co(NO_3)_2 \cdot 6H_2O$ to the LATP/EtOH on the pH and zeta potential

Fig.4

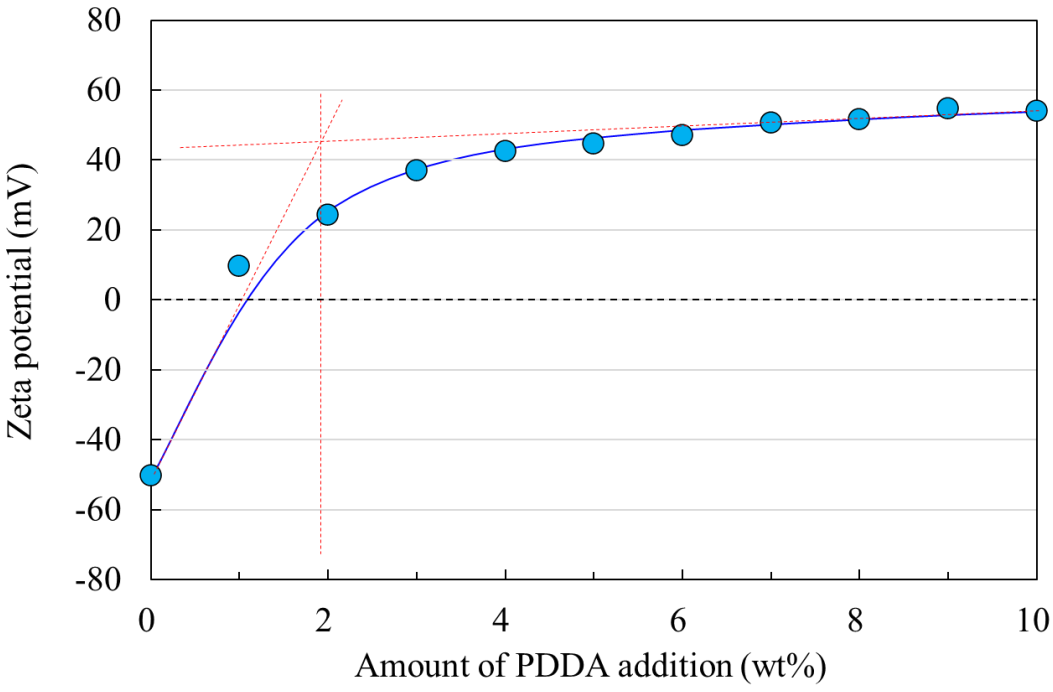

Fig. 4 The zeta potential of the LATP with varying PDDA addition amounts.

Fig.5

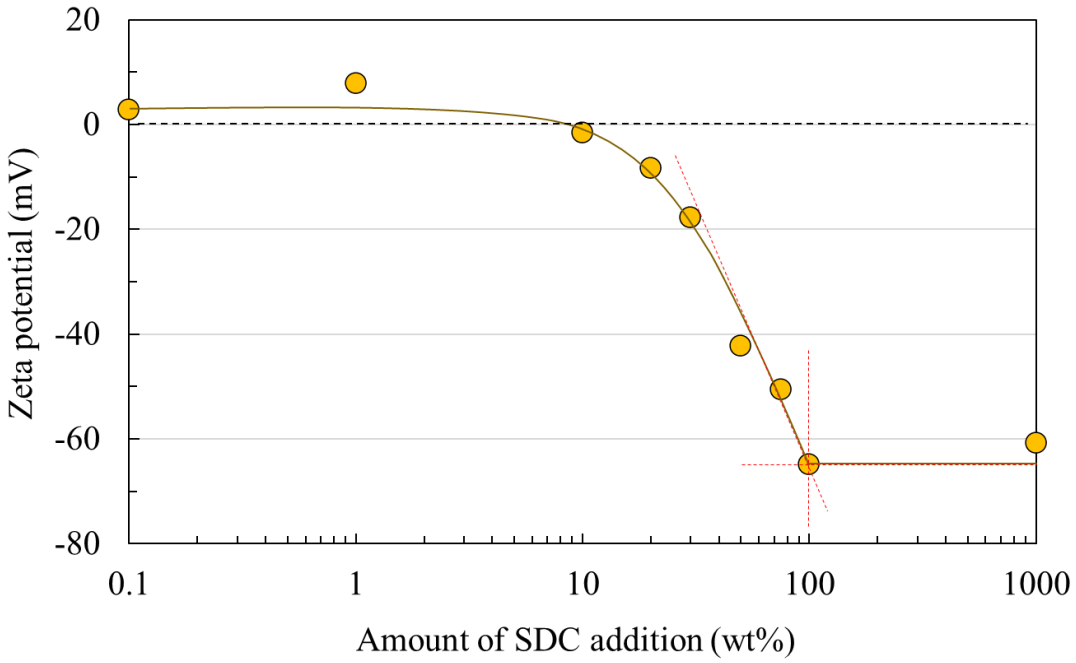

Fig.5 The zeta potential of the CNT with varying SDC addition amounts.

Fig.6

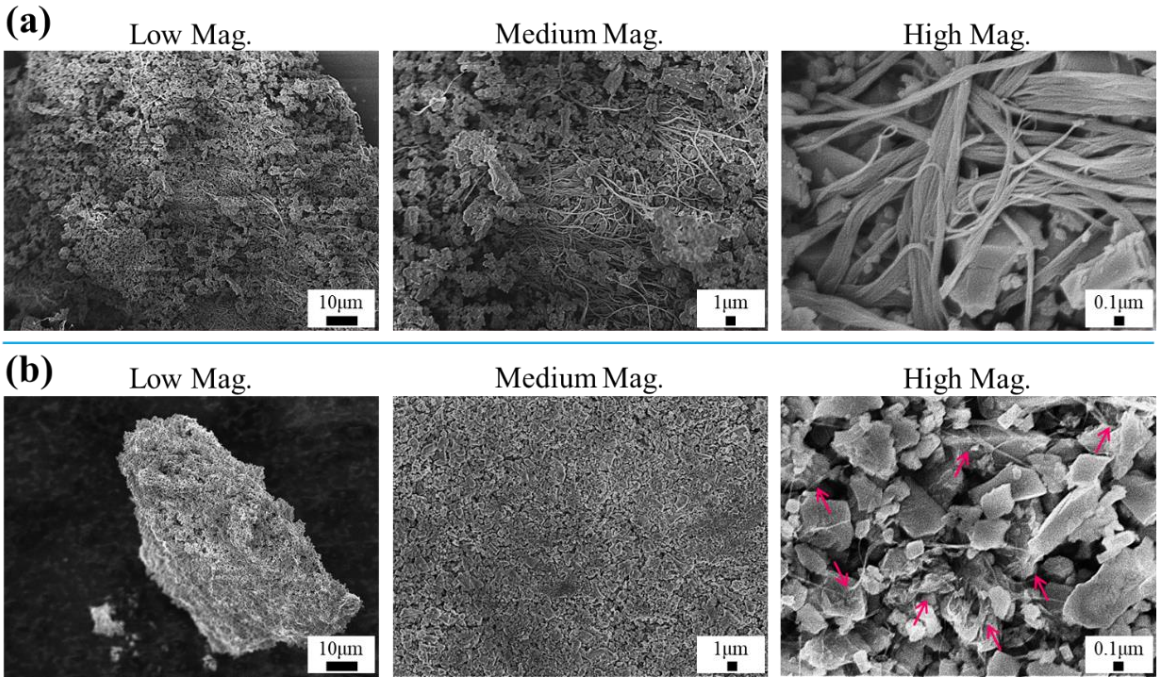

Fig.6 Morphologies of the Co-LATP and CNT composite powder at different magnifications (a) without adding PDDA and SDC, (b) with 2wt%-PDDA and 100wt%-SDC (The CNT parts are indicated by the red arrows.).

Fig.7

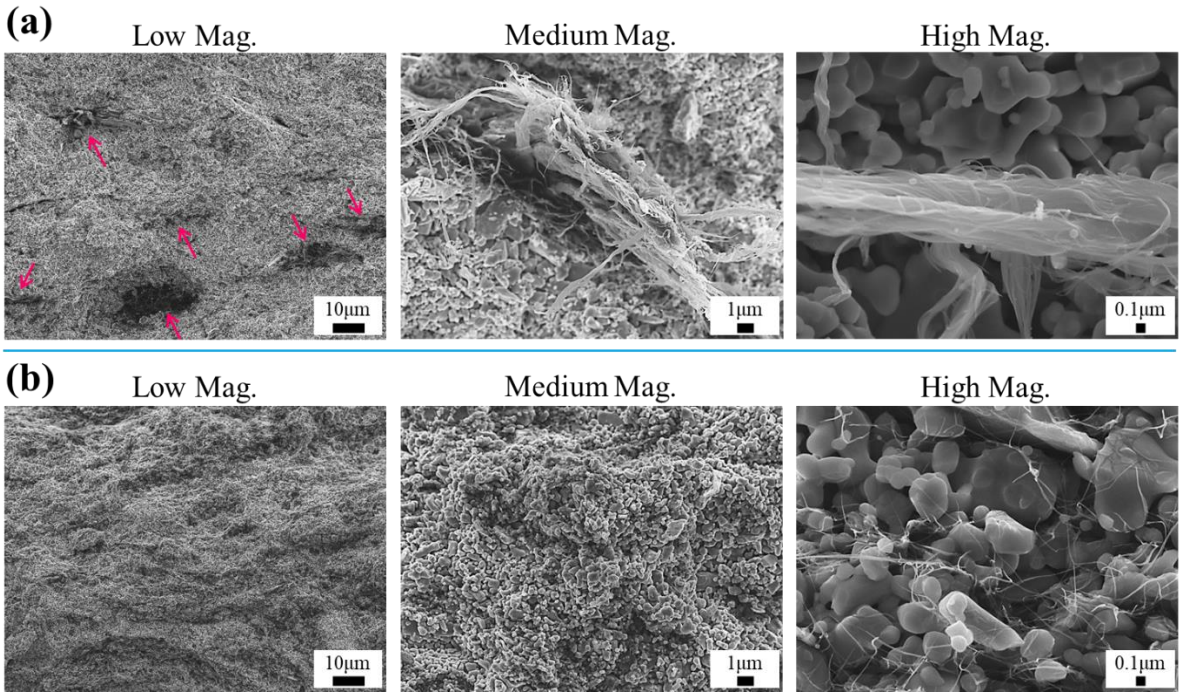

Fig. 7 The fracture surfaces of of the Co0.3-LATP and CNT composite after firing (a) without adding PDDA and SDC (The CNT parts are indicated by the red arrows.), (b) with 2wt%-PDDA and 100wt%-SDC.

Fig.8

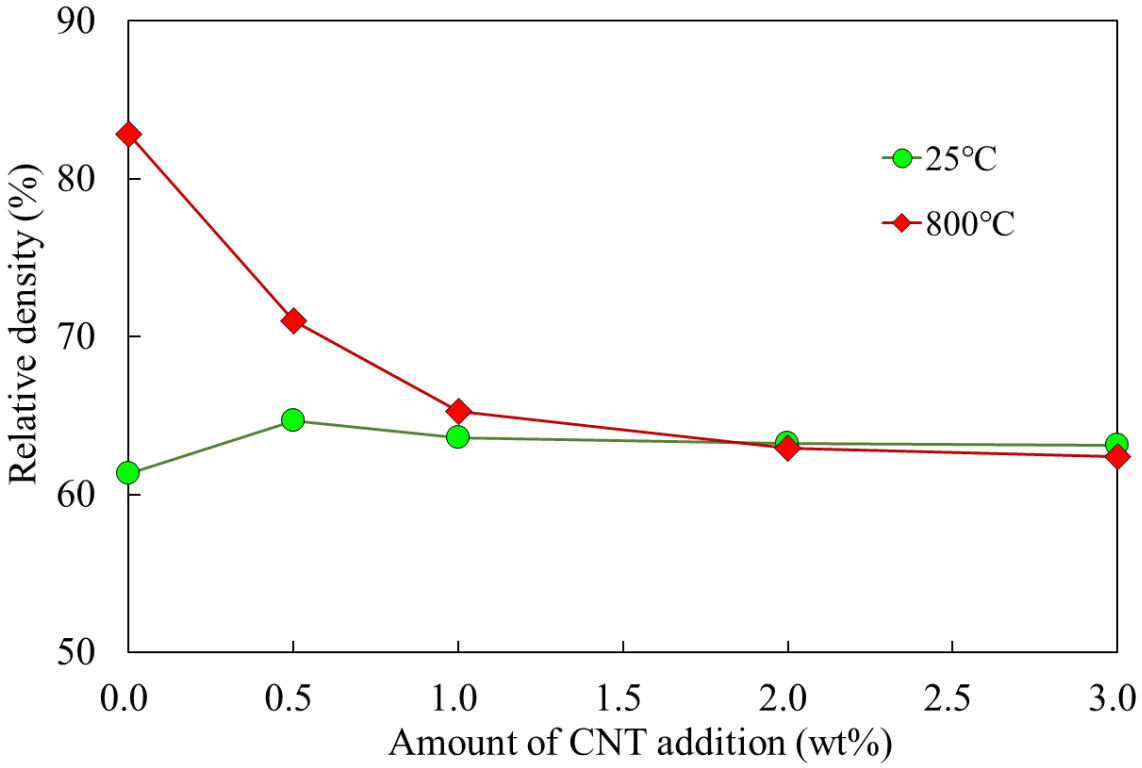

Fig. 8 The relative density of the Co0.3-LATP and CNT composite before and after firing.

Fig.9

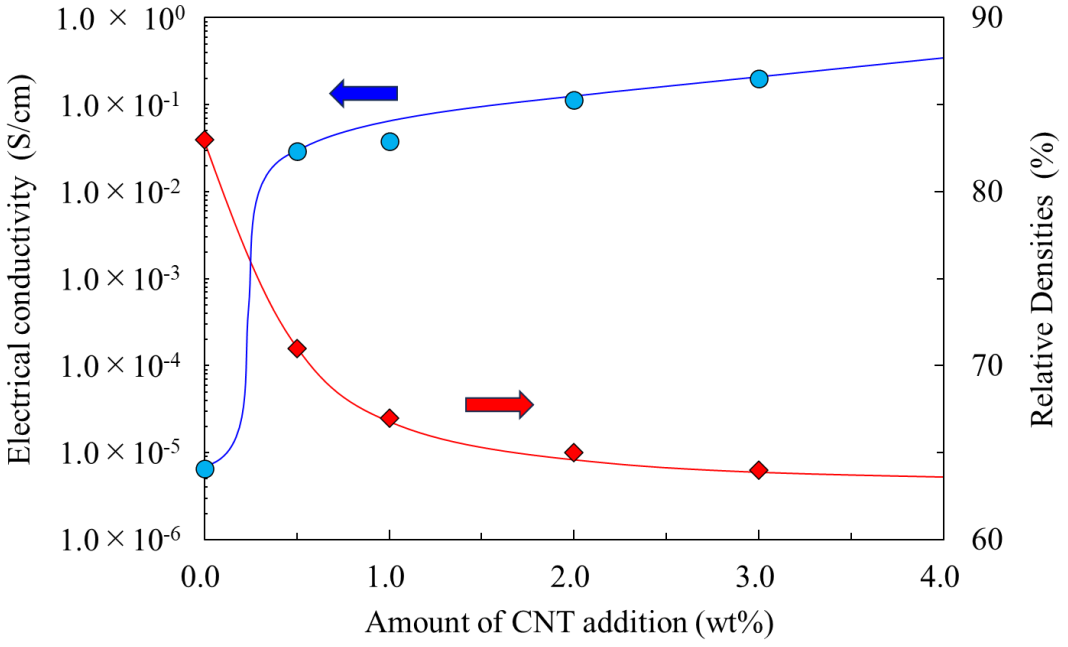

Fig. 9 The electrical conductivity and the relative density of the (Co0.3-LATP)-CNT fired bodies with various CNT additions under the addition conditions of 2 wt% PDDA and 100 wt% SDC.

Fig. 10

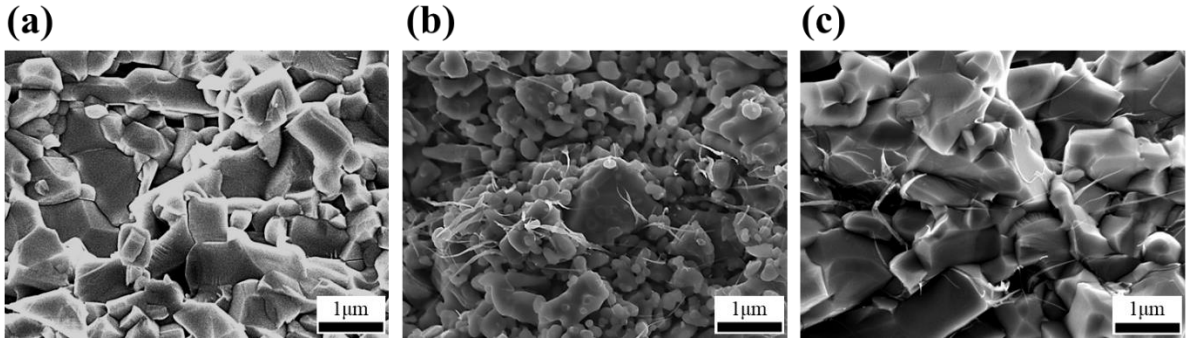

Fig. 10 The fracture surfaces of various composites after firing (a) 70vol%-LATP with 30vol%-LCP, (b) Co0.3-LATP with 0.5wt%-CNT, (c) 70vol%-(Co0.3-LATP with 0.5wt%-CNT) and with 30vol%-LCP.

Table 1

Table 1 The relative density and electrical conductivity of 70vol%-LATP with 30vol%-LCP, Co0.3-LATP with 0.5wt%-CNT and 70vol%-(Co0.3LATP with 0.5wt%-CNT) and with 30vol%-LCP.

	Relative Density (%)	Electrical Conductivity (S/cm)
70vol%-LATP with 30vol%-LCP	91	1.3×10^{-5}
Co0.3-LATP with 0.5wt%-CNT	71	2.9×10^{-5}
70vol%-(Co0.3LATP with 0.5wt%-CNT) with 30vol%-LCP	87	1.3×10^{-2}

Highlights

- Sequential particle assembling was performed to fabricate composite particle.
- Cobalt ions and CNT fibers were electrostatically adsorbed onto LATP particles.
- The zeta potential of each particle was optimized and the particles were composited.
- The finely connected path of each LATP and CNT could be formed in a sintered body.

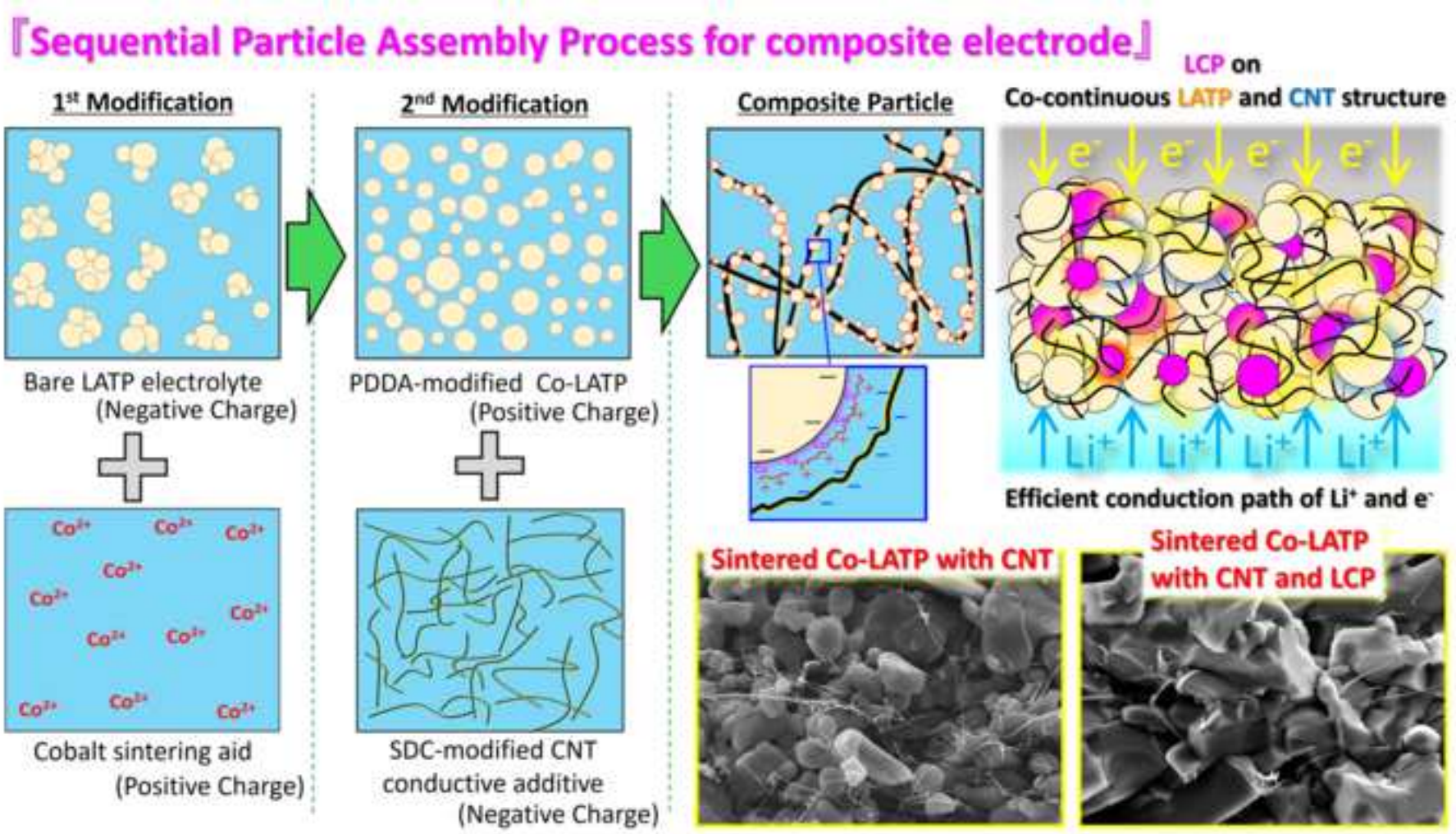

Cover Letter

Prof. Dr. Masayoshi Fuji:
Editor-in-Chief:
Advanced Powder Technology

April 3, 2024

Dear Editor,

We would like to submit our manuscript entitled, "***Design of highly-sinterable LATP-CNT composite powder by sequential particle assembly for fabrication of highly electrical-conductive composite electrodes***" to be considered for publication as an article in ***Advanced Powder Technology***.

We really appreciate the reviewers' comments, which have helped us significantly improve the paper. We made corrections to the manuscript based on the comments. Our point-by-point answer to each of the comments are attached. All the corrections based on the advice are reflected in the revised manuscript.

This paper describes in detail a sequential particle assembling process for fabricating composite particles with multiple components. Cobalt sintering aids and CNT conductive additives were sequentially and electrostatically absorbed on LATP electrolyte particles under various dispersion conditions. The effect of the particle composite conditions on the composite body's sintering ability and conductive properties was discussed. We propose the optimum microstructure of the composite particle and its particle charging conditions for obtaining a sintered composite electrode with fine connectivity of each LATP and CNT phase.

We believe that this process technology will significantly contribute to the field of powder engineering, which requires the control of the morphology of multi-component composite powders, including all-solid-state battery materials, and will be helpful to the readers of this magazine. We declare that this manuscript has not been published and is not under consideration for publication elsewhere. All the authors have read the manuscript and have approved this submission.

We look forward to hearing from you.
Sincerely,

Kento Ishii, Ph.D.
Nagoya Institute of Technology, Advanced Ceramics Research Center, 3-101-1 Honmachi, Tajimi, Gifu, 507-0033, Japan Email: < ishii.kento@nitech.ac.jp >